Chapter II

Literature Review

Thermoelectric devices are solid-state devices that convert thermal energy from a temperature gradient into electric energy (the Thompson effect), with no moving part; this makes them rugged, reliable, and quiet. They use no ozone-depleting chloroflurocarbons, potentially offering a more environmentally responsible alternative to conventional refrigeration.

When a temperature gradient is imposed on a conductor under open circuit condition (i.e. no current is allowed to flow), the creation of a steady-state potential difference between the high temperature and low temperature regions of the conductor is called Thompson effect. Consider a metal bar where one side is kept at a higher temperature than the other.

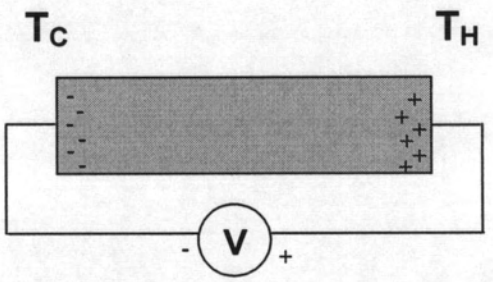

Figure 2.1: Illustation of the Thompson effect. A temperature difference in a conductor causes a net flow of electrons from the hot side (T_H) to the cold side (T_C). If the circuit is not completed, charge up occurs.

If the free electrons in the metal are considered to behave as a gas, the kinetic theory of gases predicts that the free electron in the hot side of the bar will on average have higher kinetic energy and will be moving at greater speeds than those in the cold side of the bar. As the faster moving electrons spread out, there will be a net flow of electrons from the hot side to the cold side of the bar, resulting in an accumulation of negative charge at the cold side and preventing further charge buildup (Fig.2.1).

Accumulated nagative charges also diffuse at a greater rate from the cold to the hot ends due to higher charge concentration. At equilibrium, this flow cancels out the thermal-gradient flow and the cold end will have higher electron concentration. The thermopower (α) is defined as

$$\alpha = \frac{dV}{dT} \tag{2.1}$$

Metals typically have thermopower on the order of μV/K, which are too small for most practical applications with the exception of thermocouples. Many semiconductors have much larger values of thermopower, on the order of hundreds of μV/K. Although large thermopower values are important to good thermoelectric materials, other factor is also important. Since charge carriers must move through the material to transport heat, the material should conduct electricity well. In addition, the material should act as a thermal insulator. The purpose of the device (when operated as a heat pump) is to produce a hot and cold region, so a good thermal conductor will rapidly dissipate the temperature difference established. The best thermoelectric materials involve a trade-off among the three factors, combining a high thermopower and electrical conductivity with low thermal conductivity. All three parameters are affected by the carrier concentration (n), of a solid. Electrical conductivity (σ) increases with n if mobility is constant $\sigma = ne\mu$. The thermal conductivity (k) has two components, a lattice thermal conductivity k_l and an electrical thermal conductivity k_{el} such that $k=k_l+k_{el}$. The lattice component does not significance with n; the electronic component increases with n. This relationship is displayed in Figure 2.2. These three properties were later embodied in the so-called figure-of-merit, Z. Since Z varies with temperature, a useful dimensionless figure-of-merit can be defined as ZT.

$$ZT = \frac{T\alpha^2\sigma}{k} \tag{2.2}$$

α = thermopower (μV/K)

σ = electrical conductivity (1/Ω-cm)

k = thermal conductivity (W/cmK)

T = temperature (K)

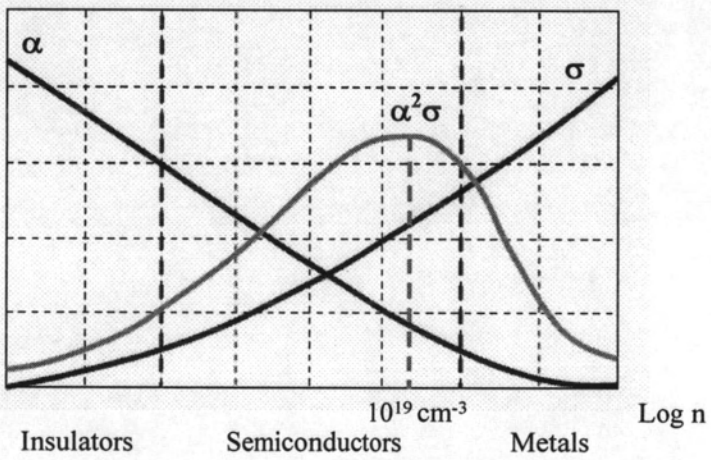

Figure 2.2: Thermopower, electrical conductivity as a function of carrier concentration [2]

The greatest Z value is obtained with a carrier concentration between 10^{18} and 10^{20} cm^{-3}. This implies that the best thermoelectric materials will be semiconductors with a relatively high carrier concentration. The choice of carrier type is also important. As mentioned above, the direction of the Thompson effect is reversed depending on whether the carriers are electrons or holes. If both carrier types are present in a material, their effect will work against each other. Semiconductors always

contain both carrier types, but often the semiconductor is intentionally doped with impurities so that one carrier type is greatly predominant. In this case, the semiconductor is said to be extrinsic. Intrinsic semiconductors, on the other hand, have roughly equal numbers of each type of carrier, causing their performance as thermoelectric materials to suffer. Extrinsic semiconductors are the better choice for thermoelectric device. Researchers are continually trying to increase the efficiency of thermoelectric materials, through the processing of existing materials or the creation of new ones. β-$FeSi_2$ is one of the attractive thermoelectric materials that can be used at high temperature in air. Figure 2.3 shows the phase diagram of Fe-Si system [3]. Semiconducting phase is orthorhombic β-$FeSi_2$ which is stable below 982°C [3]. Above this temperature it transits to the metallic phase of iron silicide consisting of tetragonal α-Fe_2Si_5 and cubic ε-FeSi. This transformation applies to subsequent heat-treated for the β-$FeSi_2$ transformation. Heat treatment about 937°C is believed to induce the peritectoid transformation α-Fe_2Si_5 + ε-FeSi → β-$FeSi_2$, which is so-called " high-temperature transformation " [4]. Heat treatment at 865°C is believed to induce the " low-temperature transformation ", with the primary transformation of α-Fe_2Si_5 → β-$FeSi_2$ + Si and the secondary transformation of Si + ε-FeSi → β-$FeSi_2$ [5].

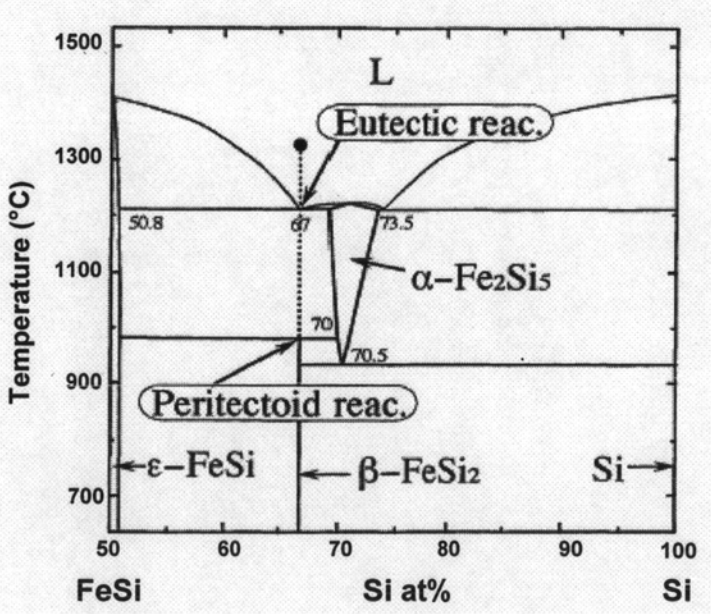

Figure 2.3: Equilibrium phase diagram of Fe-Si system

The crystal structure of ε-FeSi, α-Fe_2Si_5 and β-$FeSi_2$ are shown in Figure 2.4, ε-FeSi consisting of a cubic structure with 8 atoms in a unit cell, α-Fe_2Si_5 is a tetragonal structure with 2.87 atoms in a unit cell and β-$FeSi_2$ presents an orthorhombic structure with 48 atoms in a unit cell [3].

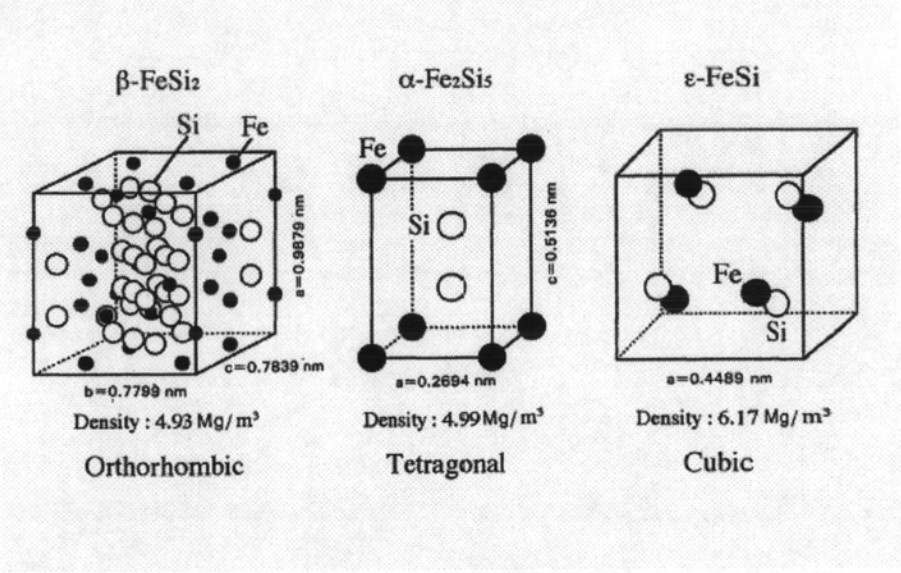

Figure 2.4: Crystal structure of β-$FeSi_2$, α-Fe_2Si_5 and ε-FeSi.

The properties of β-$FeSi_2$ make it a good thermoelectric generator material for terrestrial application

- Large seebeck coefficient, relative low electrical resistivity
- Stability with respect to oxidation, sublimation, evaporation and diffusion
- Lower cost of material than other thermoelectric materials

β-$FeSi_2$ was found possible to dope, resulting in both n and p types semiconductor. The replacement of iron by an element to its left in the periodic table e.g. Mn, Cr, Ti or other elements from this group, produces p-type material and right in the periodic table, e.g. Co, Ni, or other elements from this group, produces n-type material. The eutectic and peritectoid reactions from liquid to β-$FeSi_2$ cause difficulties to form a bulk material with a homogeneous β-$FeSi_2$. Thus in a conventional process, ingots

were grounded to fine particles and long time homogenization have been carried out to eliminate segregation. Mechanical alloying (MA) is a solid state alloying process which is suitable for the production of segregation free material with a very fine microstructure.

2.1 X-ray Diffraction (XRD)

When X-ray radiation passes through matter, the atoms absorb some of the incident radiation and re-emit it at the same frequency. There are of course losses due to scattering, but these will be neglected in the present treatment. Since the crystalline solid is a regular array of atoms in three dimensions, there will be a regularity of absorption and re-emission. The waves from individual atoms will combine in an additive fashion in some directions while annulling one another in others, depending on the phase relationships. Bragg has shown that the law governing diffraction from a crystal can be stated in the following fashion [6].

$$n\lambda = 2d\sin\Theta \tag{2.3}$$

In the Bragg equation n is the order of diffraction or the number of wavelengths difference in path for waves diffracting from successive planes. The dimension d is the distance between parallel diffraction planes, Θ is the angle between the incident beam and the diffraction plane, the term λ in the diffraction equation is the wavelength of the x-rays being used.

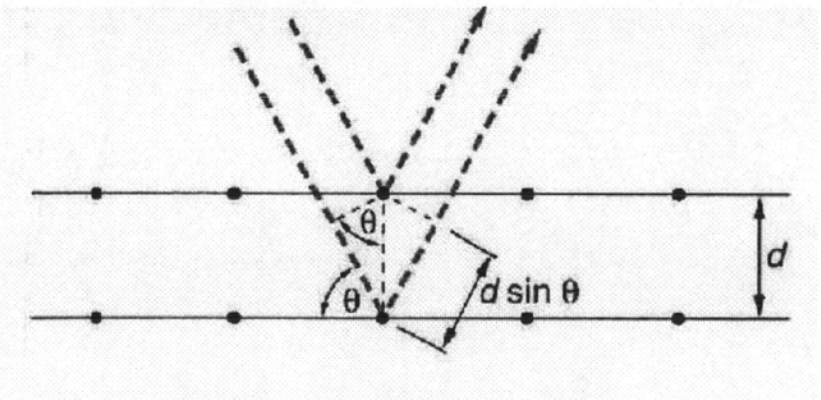

Figure 2.5: Schematic diagram for determining Bragg's law

2.2 Van der Pauw Resistivity Measurement Method

The van der Pauw method involves applying a current and measuring voltage using four small contacts on the circumference of a flat, arbitrarily shaped sample of uniform thickness. This method is particularly useful for measuring very small samples because geometric spacing of the contacts is unimportant.

Using this method, the resistivity can be derived from a total of eight measurements that are made around the periphery of the sample with the configuration shown in Figure 2.6. Once all the voltage measurements are taken, two values of resistivity, ρ_A and ρ_B are derived as follows:

$$\rho_A = \frac{\pi}{\ln 2} f_A t_s \left(\frac{V_1 + V_2 + V_3 + V_4}{4I} \right) \tag{2.4}$$

$$\rho_B = \frac{\pi}{\ln 2} f_B t_s \left(\frac{V_5 + V_6 + V_7 + V_8}{4I} \right) \tag{2.5}$$

Where ρ_A and ρ_B are volume resistivities in ohm-cm, t_s is the sample thickness in cm, V_1 -V_8 represents the voltages measured by the voltmeter, I is the current through the sample in amperes, f_A and f_B are geometrical factors based on sample symmetry.

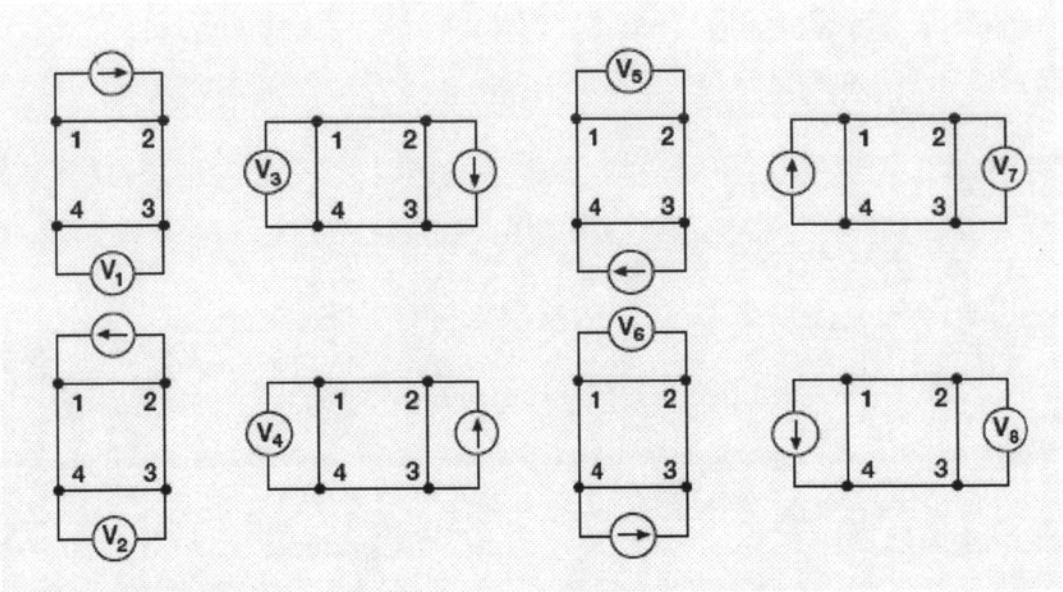

Figure 2.6: All van der Pauw resistivity configurations

f_A and f_B are related to the two resistance ratio Q_A and Q_B as shown in the following equation ($f_A = f_B = 1$) for perfect symmetry. Q_A and Q_B are calculated using the measured voltage as follows:

$$Q_A = \frac{V_1 - V_2}{V_3 - V_4}, \tag{2.6}$$

$$Q_B = \frac{V_5 - V_6}{V_7 - V_8}. \tag{2.7}$$

Also, Q and f are related as follows:

$$\frac{Q-1}{Q+1} = \frac{f}{0.693}\cosh^{-1}\left(\frac{e^{0.693/f}}{2}\right) \tag{2.8}$$

A plot of this function is shown in Figure 2.7. The value of f can be found from this plot once Q has been calculated. Once ρ_A and ρ_B are known, the average resistivity (ρ_{av}) can be determined from

$$\rho_{av} = \frac{\rho_A + \rho_B}{2}. \tag{2.9}$$

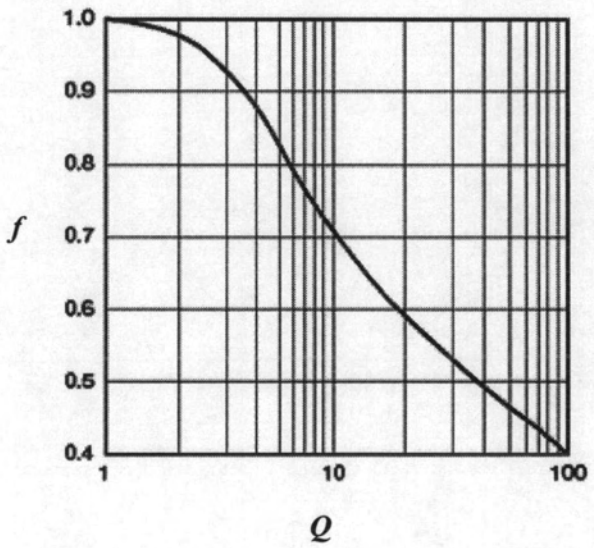

Figure 2.7: A plot of function f vs Q : the value of f can be found from this plot once Q has been calculated

2.3 Hall Effect Measurement

Hall effect measurement is important to semiconductor material characterization because from the Hall voltage, the conductivity type, carrier concentration and mobility can be derived. With an applied magnetic field, the Hall voltage can be measured using the configurations shown in Figure 2.8.

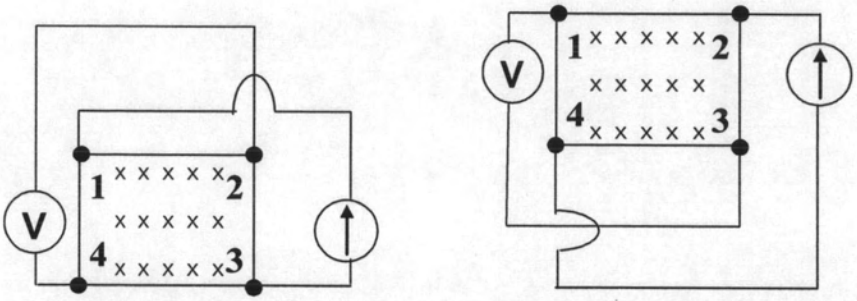

Figure 2.8: Hall voltage measurement configurations

With an applied magnetic field perpendicular to the sample and current flow between two opposite contacts, the Hall voltage is developed across the other two contacts. By field reversing both current and magnetic field direction, we have a total of eight Hall measurement configurations and the average Hall coefficient can be calculated as follows:

$$V_A = \frac{V_{24(B+)} - V_{24(B-)}}{2}, \tag{2.10}$$

$$V_B = \frac{V_{42(B+)} - V_{42(B-)}}{2}, \tag{2.11}$$

$$V_C = \frac{V_{13(B+)} - V_{13(B-)}}{2}, \tag{2.12}$$

$$V_D = \frac{V_{31(B+)} - V_{31(B-)}}{2}, \tag{2.13}$$

$$V_H = \frac{V_A + V_B + V_C + V_D}{4}, \tag{2.14}$$

$$R_H = \frac{t_s(V_H)}{IB}, \tag{2.15}$$

where R_H is Hall coefficient in cm^3/C unit, t_s is the sample thickness in cm, V_{ij} represents the voltages measured across the contact number i^{th} and j^{th}, I is the current through the sample in amperes, B is the magnetic flux in Tesla.

The sample type is determined from the sign of Hall coefficient which depends on the instrument setup. From the resistivity (ρ_{av}) and the Hall coefficient (R_H) the mobility (μ_H) can be calculated from

$$\mu_H = \frac{|R_H|}{\rho_{av}} \tag{2.16}$$

The carrier concentration is calculated from

$$n = \frac{1}{eR_H} \tag{2.17}$$

where : n is carrier concentration (cm^{-3}), e is electron charge (1.602×10^{-19} coulombs).

2.4 Preparation of Thermoelectric Films

A number of ways of fabricating thin films which have been widely adopted as a key technology in the semiconductor industries involve sputtering, ion beam deposition, molecular beam epitaxy (MBE), and activated evaporation [1].

Stoichiometric $FeSi_2$ film can be deposited in an ultra-high vacuum system by an electron beam gun onto a fused silica substrate maintained at room temperature. Thin layers of $FeSi_2$ deposited at room temperature have an amorphous structure. The layers undergo a phase transformation into crystalline β-$FeSi_2$ on heating at high temperature.

The preparation of $FeSi_2$ film by ion cluster beam (ICB) deposition was shown in Figure 2.9.

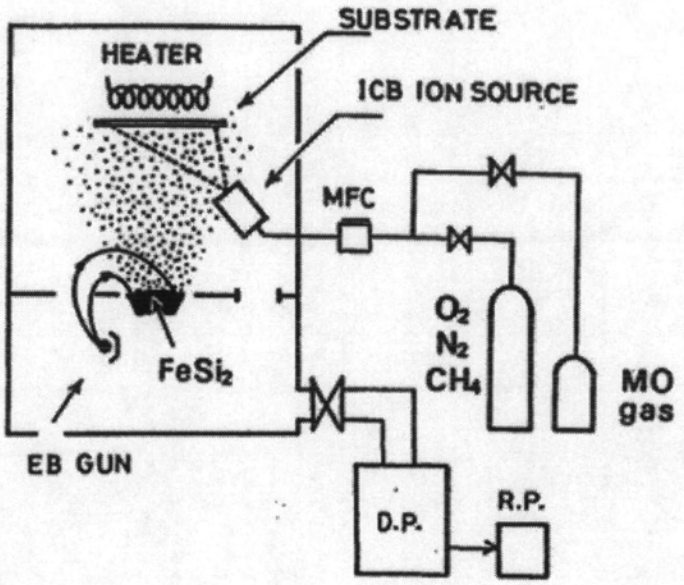

Figure 2.9: Schematic diagram of ion-assisted deposition system which is equipped with an electron beam gun and a cluster ion source [1]

This is composed of a 5-kW electron beam gun and an ion cluster beam (ICB) type sub-ion source, which is equipped to facilitate the flow of ions of a reactive gas (e.g., oxygen O_2, methane (H_4) or semiconducting gas (SiH_4) into the vacuum chamber where ion react with metal vapor evaporated from the EB-gun [1].

2.5 Mechanical Alloying

Mechanical alloying can produce new materials like amorphous powders, intermetallic materials and solid solution alloys because it relies on deformation process to mix material. During the mechanical alloying process the powder particles are trapped between colliding balls causing them to deform and mix. The ball

collisions cause fracturing and cold welding of the elementary particles. Further milling lead to a break-down and recombination of materials. Among many ball mill variations, three basic types encompass the bulk of mechanical alloying application : the attritor, the vibratory, and the planetary.

In an attritor mill, an impeller is rotated inside a tank filled with grinding balls and the materials to be processed. Microscopic fracture and cold welding occur in the powder particles trapped between the rapidly agitated balls. This type of mill has been used extensively in the production of high strength, oxide dispersion-strengthened (ODS) superalloys and MA of ductile metal powders.

The second type of mill is a vibratory mill in which a sealed vial is shaken in a complex three dimensional motions, typically a frequency of 15 to 20 Hz. Powder particles trapped between the milling balls and the vial walls undergo high-energy compressive impact forces which generate fracture, cold welding, and some heat. This type of mill more thoroughly mixes the powders and breaks down larger chunks of precursor material rather than powders which are usually used to prepare ODS superalloys by MA. This is advantageous in that reduced oxygen levels in the final consolidated alloys can be obtained compared to the use of fine powders. [1]

The third common type of ball mill is the planetary type which is used to prepare powders in this thesis. Planetary ball mill is very often used to prepare powder because very small amount of powder are required. The machine is suitable for research purposes in the laboratory. The ball mill consists of one turn disc and two or four vials (or bowls). The turn disc rotates in one direction while the vial rotates in the opposite direction. The centrifugal forces created by the rotation of the vials around its own axis together with the rotation of the turn disc are applied to the powder mixture. The powder is fractured and cold welded under high energy impact.

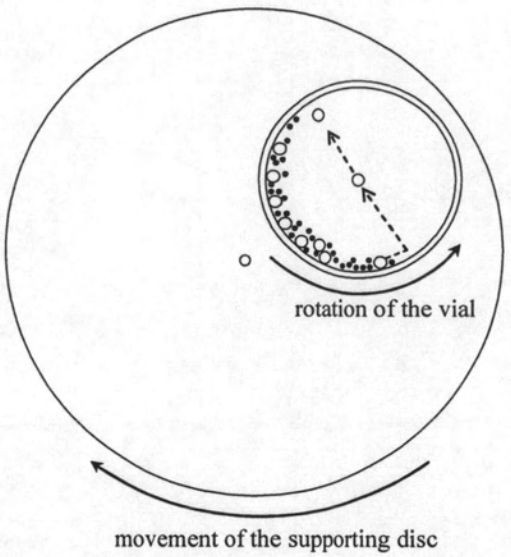

Figure 2.10: Schematic top view of motion of the balls (open circle) and powder mixture (solid circle).

Figure 2.10 shows the motions of the ball and the powder. Since the direction rotation of the vial and turn disc are opposing, the centrifugal forces produced by the rotation of the vial and disc continuously moves the powder and balls to the tangential edge of the vial. The ball impact the vial wall when it lifted and thrown across the vial to strike at the opposite wall. The impact energy of the milling is changeable by altering the rotational speed of the turn disc. The advantage of this type of ball mill is not only that high impact energy could be obtained but also high impact frequency which can shorten the duration of the mechanical alloying process. However it must be noted that because of high impact frequency, the temperature of the bowl may reach about 393 K within a short milling duration of only 30 to 60 min [7]. In cases where relatively high temperature is necessary to promote reaction rate, this may advantage to the process. Ur and Kim [5] produced n-type $Fe_{0.98}Co_{0.02}Si_2$ powder by mechanical process for 120 hours under an Ar atmosphere. For this process, stainless steel balls and powder mixtures with the weight ratio of about 20 to 1 were charged into stainless steel vial. From XRD patterns the elemental Si peaks disappeared after 72 hours of milling. The MA powders were believed to be in a metastable state presumably due to the inherently slow rate of phase transformation, which led to

processing for at least 500 hours of milling to induce β-$FeSi_2$ formation by MA. XRD analysis revealed that β-$FeSi_2$ transformation occurred at 830°C after 1 hour of annealing and the fully transformed β-$FeSi_2$ after 4 hours of annealing. The powders were successfully consolidated by vacuum hot pressing (VHP). Densities of consolidated specimens are 4.85 g/cm^3 by VHP at 1100°C and 60 MPa for 4 hours. The high density compact is shown to consist of the untransformed mixture of α-Fe_2Si_5 and ε-FeSi. It was also confirmed that the isothermal annealing near the high temperature transformation led to the distinct ε-FeSi formation. The XRD analysis after the isothermal annealing at 830°C for 4-96 hours revealed that progressive β-$FeSi_2$ transformation from α-Fe_2Si_5 and ε-FeSi took place along with the annealing time. Thermopower was increased by annealing treatment, while electrical conductivity was decreased by annealing because the metallic phase α and ε were transformed to semiconducting phases β. Min, Shim and Lee [8] prepared $(Fe_{0.95}Co_{0.05}Si_2)_xSi_2$ (x = 0.9 and 0.8) by mechanical alloying method for 50 hours of milling to sufficiently yield powders of ε-FeSi and Si phases. The pressure-resistance-sintering were employed. The sintering temperature was varied from 760-880°C at the pressure of 50 MPa. The analysis of XRD patterns of specimens showed that ε-FeSi phase remained untransformed within the matrix of β-$FeSi_2$ and Si phases when sintered at the temperature lower than 790°C. Thermopower changed negligibly with the variation of sintering temperatures. The thermopower was -183 ± 2 μVK^{-1} at room temperature. Kim et al. [9] prepared $Fe_{1-x}Co_xSi_2$ for three values of x (0.01, 0.03 and 0.05) by a powder metallurgy technique. The raw materials used in this study were Fe powder, Si chip and Co powder. The alloys were arc-melted and crushed into fine flakes. The flakes were sieved to prepare powder whose diameter was under 45 μm. The sieved powders were compacted under 625 MPa at 400°C and then sintered at temperature from 1130°C to 1200°C for 3 hours under vacuum, all sintered specimens were heat-treated at 840°C for 10 hours in a sealed quartz tube under vacuum. The thermoelectric power is measured in a temperature range from 100°C to 700°C in He atmosphere. The Co doped β-$FeSi_2$ specimens show n-type semiconductor properties. The thermoelectric power of $Fe_{0.99}Co_{0.01}Si_2$ had a maximum value at 427°C. The maximum thermoelectric powers of $Fe_{0.97}Co_{0.03}Si_2$ and $Fe_{0.95}Co_{0.05}Si_2$ are obtained at a higher temperature (477°C). Isoda et al. [10] prepared the raw materials which were electrolytic iron, silicon and cobalt. The materials required were weight out for the

compositions of $Fe_{0.985}Co_{0.015}Si_2$, and then melted by the high-frequency induction furnace in a vacuum of about 1.33×10^{-3} Pa. The excess Si content is added to compensate the Fe contamination, which cannot be avoided in the powdering process by the iron stamp and the iron ball milling. The ingots made in the above-mentioned process were crushed by a stamp mill and then grounded to the size of 1.42 μm in diameter by an iron ball mill for 50 hours. After granulation, they were cold-pressed under a pressure of 2.94×10^{2} Mpa. The green compacts were sintered in a vacuum at 1160°C for 3 hours and then finally annealed at 800°C for 200 hours. The mean particle size after sintering and annealing is 5.4 μm and 8.2 μm respectively. The thermopower (α), carrier concentration (n) and Hall mobility (μ) of Co-doped n-type $FeSi_2$ at room temperature is -360 μV/K, 1.8×10^{20} cm^{-3} and 0.7 $cm^2V^{-1}s^{-1}$ respectively.

Preparing doped-$FeSi_2$ from the conventional ingot technology cannot produce a homogeneous dopant distribution in the matrix [5]. The dopants iron atoms ($Fe_{1-x}Co_xSi_2$) for n-type which were melted. The ingot can be crushed and the lumps be grounded in a ball mill. The powder consists of the untransformed mixture of α-Fe_2Si_5 and ε-FeSi. The densification of powder can be performed either by cold pressing with subsequent sintering treatment or by hot pressing. To obtain β-$FeSi_2$ a phase transition has to be induced after sintering by annealing. Electronic transport parameters and thermoelectric properties of literature are shown in Table 2.1.

Method	Hot-press 1100°C Heat-treat 830°C	Hot-press 760-880°C	Hot-press 400°C Sinter 1130°C Heat-treat 840°C	Cold-press Sinter 1160°C Heat-treat 800°C
Electron conductivity ($\Omega^{-1}cm^{-1}$)	10-30	62-109	50-150	20
Electron mobility (cm^2/Vs)	3-400	1.2-1.8	-	0.7
Electron concentration (cm^{-3})	5×10^{17}-2×10^{19}	3.1×10^{20} - 4×10^{20}	-	1.8×10^{20}
Seebeck coefficient ($\mu V/K$)	(-100)-(-300)	-183±2	(-200)-(-300)	-360
Reference	[5]	[8]	[9]	[10]

Table 2.1: Electronic transport and thermoelectric property of references